

# Modeling the hygro-mechanical response of quasi-brittle materials

P. Moonen & L.J. Sluys

*Department of Civil Engineering and Geosciences, Delft University of Technology, Delft, The Netherlands.*

J. Carmeliet

*Laboratory of Building Physics, Department of Civil Engineering, Katholieke Universiteit Leuven, Belgium.*

**ABSTRACT:** Performing accurate, large scale computations requires a model formulated on the macro-scale, but involving relevant physical phenomena taking place on the lower scales. In the present paper, a macroscopic framework for the simulation of the hygro-mechanical response of quasi-brittle porous materials is proposed. The model employs the partition of unity (PU) concept and introduces a new generic cohesive law. With the PU concept, crack growth can be studied on relatively coarse meshes. The new cohesive law allows extending most continuum models to a discontinuous framework, hereby adding the effect of macro-crack formation by the growth en coalescence of micro-defects. The capabilities of the model are illustrated by means of a simple poromechanical material model. It is shown that good correspondence with experimental results is already obtained based on linear elasticity and a perfectly brittle response. It can be expected that the use of more sophisticated material models will lead to better results.

## 1 INTRODUCTION

In the past decades, significant progress has been made in computational modeling of damage and fracture processes in quasi-brittle materials such as concrete and masonry. Most of the available models are continuum models which require very fine finite element meshes in the vicinity of a crack or localization zone. Discrete models are consistent with the physical observation of a discrete crack as a displacement jump across a discontinuity surface. The extended finite element approach belongs to this class of models (e.g. Moës et al. 1999; Belytschko et al. 1999; Dolbow et al. 2000; Wells et al. 2001). In this formulation, cracks are not restricted to the finite element boundaries; instead, they can freely run through the finite element mesh. As a result, coarser meshes can be used, rendering these models suitable for larger scale computations. However, an embedded discontinuity in a coarse mesh cannot capture the actual tortuosity of the real crack surface and the resulting frictional and hooking resistance, nor can it accurately represent the energy consumed by micro-crack branching prior to the formation of the macro-crack. A better characterization of the whole failure process can be achieved by combining continuous and discontinuous theories into a global framework.

This idea has been successfully pursued by many authors (e.g. Ren et al. 1997; Jirásek et al. 2001; Oliver et al. 2002; Simone et al. 2003), nevertheless some issues remain. It is for example not clear when

a discrete crack should be introduced. Some authors introduce a traction-free discontinuity at the final stages of failure. In this case the continuum model governs the softening behavior (e.g. Simone et al. 2003). Other authors make use of the cohesive zone assumption (Dugdale 1960; Barenblatt 1962). Here a traction-separation model governs the non-linear behavior in the fracture process zone and the continuum can remain elastic at all times (e.g. Wells et al. 2001). Both approaches have in common that a single moment exists at which the continuous model is replaced by a discontinuous model. The distinct feature of the model proposed in the present paper is that this transition takes place gradually. A damage-type cohesive law allows using the constitutive model for the continuum in the undamaged material bridges at the process zone, whereas the damaged part of the crack is traction-free. As damage grows, material bridges are broken and a macro-crack is formed. The cohesive zone model is formulated irrespective of the (continuum) material model.

The paper starts with a review of the basic equations of the extended finite element approach. Next, the governing equations for the cohesive zone model are derived. Issues like damage growth and crack initiation and propagation are discussed and a return mapping algorithm is proposed. Next, a simple poromechanical continuum model is presented. Finally, simulations of four-point bending tests are conducted and compared to experimental results, and differences between both are discussed.

## 2 NUMERICAL MODEL

### 2.1 Strong discontinuities

Cracking is modeled using a discrete approach: strong (displacement) discontinuities are embedded in finite elements (Figure 1a).

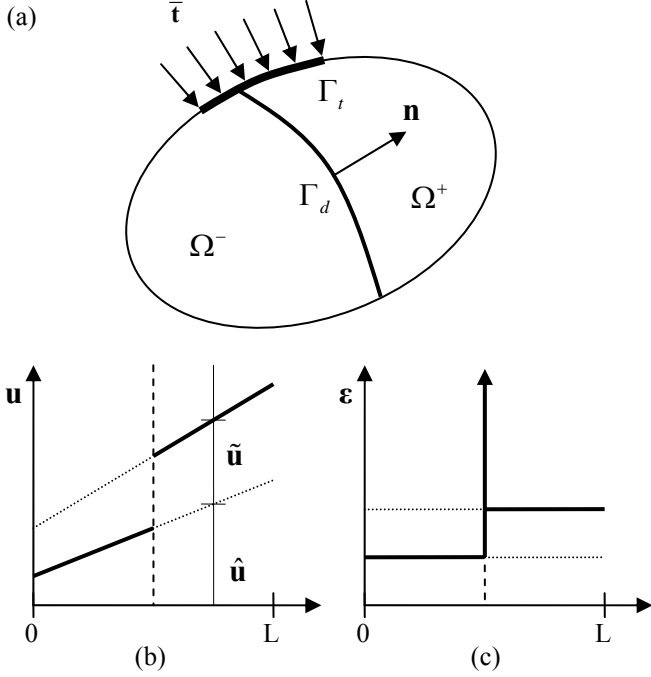


Figure 1: (a) Body  $\Omega$  crossed by a displacement discontinuity. (b) Schematic representation of the displacement field and (c) the corresponding strain field of a crossed 1D element.

The total displacement field (Figure 1b) of a body  $\Omega$  crossed by a displacement discontinuity is given by

$$\mathbf{u} = \hat{\mathbf{u}} + H_{\Gamma_d} \tilde{\mathbf{u}} \quad (1)$$

where  $\hat{\mathbf{u}}$  and  $\tilde{\mathbf{u}}$  are smooth, continuous functions on  $\Omega$  and  $H_{\Gamma_d}$  is the Heaviside step function corresponding to and centered at the discontinuity  $\Gamma_d$ . The Heaviside function is equal to one for all points  $x \in \Omega^+$  and zero for all other points  $x \in \Omega^-$ .

The strain field (Figure 1c) can be found by taking the symmetric gradient of the displacement field:

$$\boldsymbol{\varepsilon} = \nabla^s \mathbf{u} = \nabla^s \hat{\mathbf{u}} + H_{\Gamma_d} \nabla^s \tilde{\mathbf{u}} + \delta_{\Gamma_d} (\tilde{\mathbf{u}} \otimes \mathbf{n})^s \quad (2)$$

where  $\mathbf{n}$  is the normal to the discontinuity and  $\delta_{\Gamma_d}$  is the Dirac delta distribution, centered at the discontinuity. The Dirac delta distribution is the derivative of the Heaviside step function and is nonzero only for the points on the discontinuity.

### 2.2 Discrete constitutive model

#### 2.2.1 Cohesive zone assumption

Dugdale (1960) and Barenblatt (1962) proposed to model the inelastic deformations ahead of a crack as

cohesive forces acting on a fictitious extension of the crack (Figure 2). Moving along the fictional crack towards the actual crack tip, the traction forces on the crack faces reduce gradually from their maximal value to zero. As a result, the stress singularity at the crack tip, predicted by Linear Elastic Fracture Mechanics (LEFM), is removed.

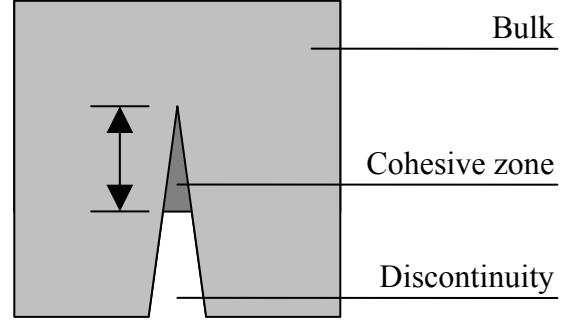


Figure 2: Schematic representation of the cohesive zone concept: inelastic deformations ahead of the crack tip are modeled as cohesive forces acting on a fictitious extension of the crack.

In the present paper, the cohesive zone will only account for the effects of damage. The proposed methodology can easily be extended to incorporate other types of inelastic behavior as well (e.g. plasticity).

#### 2.2.2 Constitutive equation for the cohesive zone

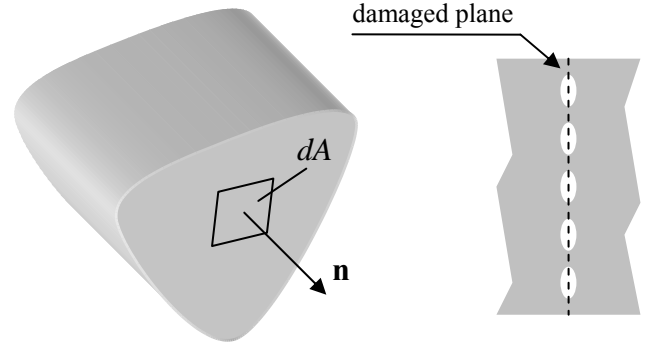


Figure 3: Schematic representation of an infinitesimal part of a plane with normal  $\mathbf{n}$  in a structure or structural component (left) and of the cohesive zone with approximately 60% in-plane micro-damage (right).

Consider an infinitesimal part of a plane with unit normal  $\mathbf{n}$  in a structure or structural component (Figure 3, left). The stresses or, more precisely, tractions acting on this plane are obtained as

$$\mathbf{t} = \boldsymbol{\sigma} \mathbf{n} \quad (3)$$

where  $\boldsymbol{\sigma}$  is the second order continuum stress tensor. Suppose that micro-cracks and -voids start to grow on this infinitesimal plane. In that case, we can quantify the ratio between the damaged and the total area with a scalar damage variable  $d$ , ranging from zero to one (Figure 3, right). Zero damage corresponds to the bulk material, whereas  $d$  equals one upon complete separation along the crack plane. The

bulk material will in general include pores, deficiencies and irregularities. All these ‘imperfections’ are randomly distributed in the material. As a result, they are not considered as ‘damage’ but rather as a characteristic of the continuum.

Tractions can only be transferred through the undamaged material bonds. According to Saint-Venant’s principle, the micro-voids and -cracks influence the stress field in the surrounding continuum material only locally. If the micro-voids and -cracks grow and coalesce into macro-cracks, the surrounding material will relax and all stresses will vanish. Hence, it is reasonable to assume that the effective tractions in the material bonds  $\mathbf{t}_{eff}$ , integrated over the infinitesimal area  $dA$ , must equal the homogenized stresses in the surrounding continuum, projected on the plane and integrated over the same area (Eq. 4). Herein, inertia-effects are disregarded for simplicity.

$$\boldsymbol{\sigma} \mathbf{n} dA = \mathbf{t}_{eff} (1-d) dA \text{ for } 0 \leq d \leq 1 \quad (4)$$

Before any damage occurs, the effective stresses equal the homogenized stresses (Eq. 4 with  $d = 0$ ). As damage grows, the active area decreases and the effective tractions increase. Hereby, the redistribution of the tractions causes additional deformations in the undamaged material bonds, a process often termed as localization. The corresponding strain field is given by equation (2), where the first two terms on the right hand side can be considered as continuum strains and where the third term describes the localization, here modeled as separation of the crack surfaces. Similarly, the effective stresses in the undamaged material bonds can be expressed as a sum of a continuum and a discrete contribution:

$$\mathbf{t}_{eff} = \boldsymbol{\sigma} \mathbf{n} + \mathbf{Q} [[\tilde{\mathbf{u}}]] \quad (5)$$

where  $\mathbf{Q} = \mathbf{n} \mathbf{C} \mathbf{n}$  is the acoustic tensor, with  $\mathbf{C}$  a 4<sup>th</sup> order constitutive tensor describing the constitutive behavior of the bulk material, and  $[[\tilde{\mathbf{u}}]]$  is the width of the discontinuity. The first term of equation (5) describes the tractions that act on the plane if damage were absent. The second term corresponds to the redistributed tractions due to the actual damage.

Combining equations (3-5) finally yields the constitutive equation for the cohesive zone:

$$\mathbf{t} = (1-d) [\boldsymbol{\sigma} \mathbf{n} + \mathbf{Q} [[\tilde{\mathbf{u}}]]] \quad (6)$$

Equation (6) represents the gradual degradation from a continuum to a localized state. A graphical interpretation is given in Figure 4.

Upon initiation of the crack, the crack width and the damage variable equal zero and Eq. (3) is recovered: the material behaves as if no discontinuity were present.

As damage grows, the relative contribution of the discrete component of the total traction gains importance over the continuum component. For softening materials, the total traction will generally decrease with increasing damage. The limit case is adequately illustrated by a force-driven (uni-axial) tensile test on a bar with limited cross-section. Here, additional damage will cause additional deformations, but will not cause stress relaxation. Hence the total load will be carried up to the moment that rupture occurs and the material suddenly relaxes. For hardening materials the same scenario applies, but the total tractions progressively increase up to the point where failure occurs. At rupture, the damage variable becomes one, and the traction forces become zero (Eq. 6). This corresponds to a traction-free discontinuity.

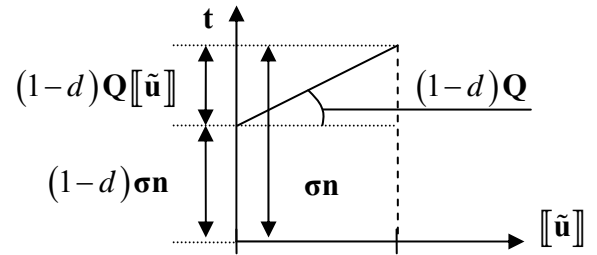


Figure 4: Schematic representation of the components of the traction force vector in a crossed 1D-body  $\Omega$ .

### 2.2.3 Damage evolution

So far we have not discussed when and at which rate the damage should grow. The proposed discrete constitutive equation needs to be supplemented with a proper damage criterion and a suitable damage evolution law.

Criteria for damage growth are either stress-based or strain-based (Simo et al. 1987) and require the definition of an effective stress or strain, respectively. Considering that (1) the discrete law (Eq. 6) crucially depends on the equilibrium between the effective tractions in the undamaged material bridges and the homogenized stresses in the surrounding continuum matrix, and that (2) the corresponding strain field (Eq. 2) is unbounded due to the presence of the Dirac delta function, it is clear that a stress-based damage criterion is preferred. A rankine-type equation is adopted:

$$f(\mathbf{t}_{eff}, d) = t_{eq} - \kappa \leq 0 \quad (7)$$

in which  $t_{eq}(\mathbf{t}_{eff})$  is an equivalent traction, expressed in function of the effective tractions, and  $\kappa(d)$  is the residual strength of the damaged material. For mode I dominated failure, the following expression for the equivalent traction is found suitable:

$$t_{eq} = \mathbf{t}_{eff} \cdot \mathbf{n} = (\boldsymbol{\sigma} \mathbf{n} + \mathbf{Q} [[\tilde{\mathbf{u}}]]) \cdot \mathbf{n} \quad (8)$$

The simplest expression for  $\kappa$  is given by

$$\kappa(d) = f_t + H(d) \quad (9)$$

with  $f_t$  the tensile strength of the bulk material and  $H(d)$  a hardening (or softening) function.

Damage evolution is governed by the Kuhn-Tucker conditions:

$$\dot{d} \geq 0, \quad f \leq 0, \quad \dot{d} f = 0 \quad (10)$$

supplemented with the consistency condition

$$\dot{d} \dot{f} = 0 \quad (11)$$

Instead of determining the damage rate from the consistency condition, we propose to update the damage variable based on energy considerations. If the damage criterion is violated, the excess elastic energy stored in the system must be consumed by opening the crack. Equating (1) the elastic energy and (2) the work done by the traction forces and performing some straightforward algebraic operations yields the following return mapping algorithm

$$d^{t+dt} = \frac{(\boldsymbol{\sigma} \cdot \boldsymbol{\sigma}) + 2(\boldsymbol{\sigma} \cdot \mathbf{Q}[\tilde{\mathbf{u}}]) - (1-d^t)^2 \kappa^2}{(\boldsymbol{\sigma} \cdot \boldsymbol{\sigma}) + 2(\boldsymbol{\sigma} \cdot \mathbf{Q}[\tilde{\mathbf{u}}]) + (1-d^t)^2 \kappa^2} \quad (12)$$

If the obtained damage variable violates the Kuhn-Tucker conditions, the previous value should be kept. Upon convergence of the iterative procedure, the damage variable, crack width and continuum stress field are updated.

#### 2.2.4 The initiation and propagation rule

Finally we need to define when a discontinuity should initiate or propagate. We have already shown that upon crack initiation, the discrete constitutive equation (Eq. 6) reduces to the traction equilibrium on the potential crack plane (Eq. 3). In the same line of reasoning, the discrete damage criterion (Eq. 7) corresponds to the following initiation criterion:

$$f = \sigma_i - \kappa \leq 0 \quad (13)$$

with  $\sigma_i$  the  $i^{\text{th}}$  eigenstress and  $\kappa = f_t + H(d=0)$ . If equation (13) is violated, a new crack segment must be introduced with the normal pointing in the (critical) principal stress direction.

It is recommended to determine the direction of the discontinuity based on the non-local stress tensor, calculated as a weighted average of stresses using a Gaussian weighting function (Jirasek 1998):

$$\bar{\boldsymbol{\sigma}} = \frac{\int_{\Omega} w \boldsymbol{\sigma} d\Omega}{\int_{\Omega} w d\Omega} \quad \text{with} \quad w = \frac{1}{(2\pi)^{3/2} l^3} \exp\left(-\frac{r^2}{2l^2}\right) \quad (14)$$

where  $r$  is the distance to the crack tip and  $l$  the influence length, taken approximately equal to three times the element size (Wells et al. 2001).

### 2.3 A simple hygro-mechanical material model

The framework has been formulated irrespective of the constitutive model used for the continuum. To illustrate the inherent capability of the model to extend the range of applicability of even the simplest constitutive equation, and to demonstrate that the framework can deal with arbitrary material models, it was chosen to study the hygro-mechanical response of porous materials.

The capillary pressures in the material matrix generate additional internal stresses of which the magnitude can be estimated based on the elastic effective stress concept (Coussy, 1995).

The total stress tensor is defined as

$$\boldsymbol{\sigma} = \mathbf{C}\boldsymbol{\varepsilon} + b \left( \int_{p_{c,ref}}^{p_c} S(p_c) dp_c \right) \mathbf{I} \quad (15)$$

where  $\mathbf{C}$  is the 4<sup>th</sup> order Cauchy stress tensor,  $\boldsymbol{\varepsilon}$  the 2<sup>nd</sup> order strain tensor,  $b = 1 - K/K_s$  is the biot coefficient (assumed to be constant), with  $K$  the bulk modulus of the grain material and  $K_s$  the bulk modulus of the skeleton,  $\mathbf{I}$  the second order unity tensor and  $S(p_c)$  the moisture retention curve. Since moisture saturation is hardly affected by strain for quasi brittle porous materials, we assume the degree of moisture saturation  $S$  to be only a function of the capillary pressure  $p_c$ . For unsaturated conditions, the capillary pressure is defined as

$$p_c = p_l - p_g < 0 \quad (16)$$

with  $p_l$  the liquid pressure and  $p_g$  the gas pressure.

The saturation curve  $S(p_c)$  can experimentally be obtained by a combination of different techniques (Roels et al., 2001) and described in analytical form by a sum of power functions (Durner, 1994):

$$S(p_c) = \frac{w(p_c)}{w_{sat}} = \sum_{i=1}^{nps} l_i \left( 1 + (-c_i p_c)^{n_i} \right)^{-m_i} \quad (17)$$

with  $w(p_c)$  being the moisture content as a function of capillary pressure and  $w_{sat}$  the moisture content at saturation,  $nps$  is the number of pore systems in the material,  $l_i$  are the weighting factors ( $0 < l_i \leq 1$ ,  $\sum_{i=1}^{nps} l_i = 1$ ) and  $c_i$ ,  $n_i$  and  $m_i = 1 - 1/n_i$  model parameters related to the  $i^{\text{th}}$  pore system. The integral of the moisture saturation curve is calculated from a reference capillary pressure  $p_{c,ref}$ , theoretically equal to  $-\infty$ . In practice a sufficiently large negative value (e.g.  $-10^{12}$  Pa) is used. Note that the hygric stress contribution is assumed to be hydrostatic.

### 3 EXPERIMENTAL VALIDATION

#### 3.1 Experimental set-up

Four-point bending tests were performed on dry ( $S=0\%$ ) and wet ( $S=100\%$ ) notched samples of Meule sandstone. The beam had a length of 0.24 m and cross-sectional dimensions 0.048 m x 0.024 m (height x depth). Two different notch sizes were considered. Both had the same width of 0.004 m and a circular tip. The total notch depth was 0.008 m for the small notch and 0.016 m for the large notch. The distance between the two supports was 0.2 m and between the loading points 0.1 m. The tests were conducted under displacement control. To this end, an extensometer with measurement basis of 0.0125 m was placed over the notch, on the bottom surface of the sample. The load was controlled as such that the crack mouth opening displacement (CMOD) would increase with a constant rate of 0.1 mm/min. A sampling rate of 20 pts/s was chosen.

#### 3.2 Numerical simulations

The tests were simulated with the model described in the previous sections. The simulations were performed in 2D, using both the plane stress and the plane strain assumption. Due to the utilization of the partition of unity method, the fracturing process is, by definition, independent of the mesh size. Structured meshes were used (Figure 5). The mesh for the sample with the small notch consisted of 2666 bilinear 4-noded quadrilateral elements, resulting in 2786 nodes. The sample with the large notch was meshed with 2626 elements, using 2754 nodes. A time step of 1 second was selected. The maximum number of new crack segments in a time step was restricted to 5, but with the selected mesh and time step, this limit was never reached. Crack path continuity was imposed.

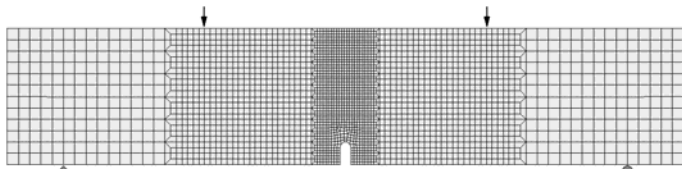


Figure 5: Representative mesh used in the simulations, with indication of the boundary conditions.

Carmeliet and Van Den Abeele (2004) showed that the elastic behavior of Berea Sandstone is strongly influenced by moisture saturation, especially in the lower saturation range. Meule sandstone exhibits a similar behavior. In Roels et al. (2006) a simplified expression is used to describe the dependency of the Young's modulus on saturation:

$$E(S) = E_{S=0} + (E_{S=1} - E_{S=0})S^{1/2} \quad (18)$$

with  $E_{S=0}$  being the Young's modulus at dry state ( $S=0$ ) and  $E_{S=1}$  the Young's modulus at vacuum saturation state ( $S=1$ ). If the critical strain  $\varepsilon_{cr}$  in the material is assumed to be independent of the saturation level, the dependency of the tensile strength on the degree of moisture content reads

$$f_t(S) = E(S)\varepsilon_{cr} \quad (19)$$

which means that tensile strength varies in the porous medium in the case of a non-uniform moisture distribution. Realistic moisture patterns can be obtained by coupling the mechanical model to a moisture transport model as described in Roels et al. 2006.

The mechanical and hygric material properties are summarized in Table 1. The hardening/softening parameter in equation (9) is not used in the simulations to simplify the interpretation of the results.

Table 1. Material properties used in the simulations.

Property	Units	Value	
$E_{S=0}$	(GPa)	14.0	
$E_{S=1}$	(GPa)	6.3	
$\nu$	(-)	0.3	
$f_t$	(MPa)	3.0	
$b$	(-)	0.6	
$l_{1,2}$	(-)	0.30	0.70
$c_{1,2}$	(-)	$1.25e-5$	$1.80e-5$
$n_{1,2}$	(-)	1.65	6.00

#### 3.3 Discussion of the results

Figure 6 shows the load-strain diagram for the dry specimens ( $p_c \approx -10^{10}$  Pa) with the small notch. Experimental data are shown with solid grey lines and simulation results with dashed black lines. All loads have been divided by the width of the sample to exclude the effect of sample thickness. The strain is obtained by dividing CMOD by the length of the measurement basis of the extensometer.

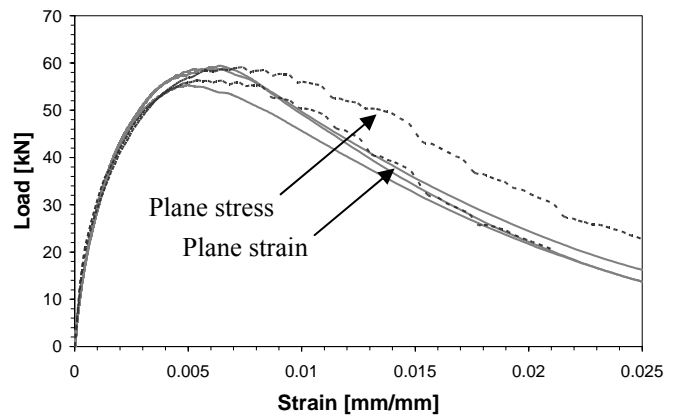


Figure 6: Load-strain curve of a notched dry beam (notch depth 8 mm) subjected to a four-point bending test. Experimental data are indicated with solid grey lines, simulation results with dashed black lines.

From Figure 6 it is clear that the proposed model captures the loading branch, the peak load and the softening branch well. The differences between plane stress and plane strain only become apparent in the descending branch. The plane stress model results in a larger cohesive zone and hence the residual strength of the model is higher.

The experimental results and simulations for the dry samples with the large notch are shown in Figure 7. Already in the second part of the loading branch, the simulations start drifting away from the experimental curves. The relative difference increases with increasing strain, both under the plane stress and the plane strain assumption. Nevertheless, the peak load is still reproduced well. The difference can partially be attributed to the boundary conditions. In the simulations only the vertical displacements at the supports have been prohibited. No limits are imposed to the horizontal displacements. In the real test set up the sample is placed on two rolling-supports. They augment the structural stiffness in two ways. On the one hand the supports hinder the bending of the beam due to their rotational capacity and introduce horizontal stresses in the sample. On the other hand their spacing is fixed in time, and does not grow like in the simulation. A third factor contributing to the difference between measurements and simulations is related to the implementation of the crack initiation and propagation rule. When the initiation criterion (Eq. 13) is met in any of the integration points in an element, a discontinuity segment is introduced through the entire element. As a result the discontinuity will grow in discrete steps. This is the reason for the “bumps” in the softening branches of all simulations. In general these bumps do not influence the structural behavior, however for a sample with a notch over 1/3 of the total height, the introduction of the first crack segment causes a noteworthy decrease of the cross-sectional area, speeding up the damage process.

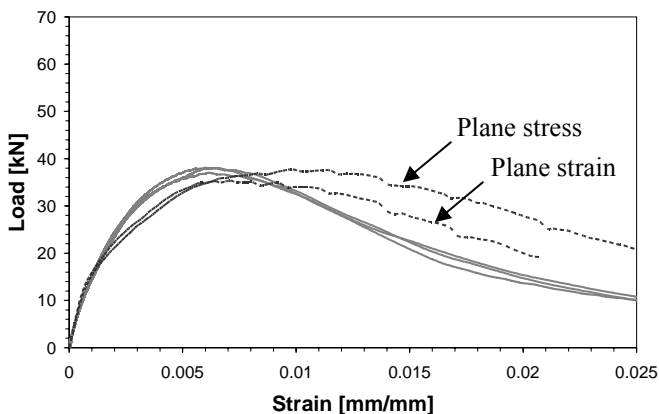


Figure 7: Load-strain curve of a notched dry beam (notch depth 16 mm) subjected to a four-point bending test. Experimental data are indicated with solid grey lines, simulation results with dashed black lines.

It should be noted that the observed softening branch results from an elasto-perfectly plastic Rankine criterion since the softening variable (Eq. 9) is not used.

Finally the four-point bending test on saturated samples ( $p_c \approx -10$  Pa) with a small notch is studied (Figure 8). The presence of moisture manifests itself in a decrease in stiffness and a reduction of the tensile strength. The poromechanical model overpredicts the initial stiffness but the peak load and the softening branch show good agreement. Since tensile strength and Young’s modulus are linked by equation (19), obtaining a better match for the initial stiffness will result in an inferior correspondence of the peak load. Consequently, the existence of a moisture-independent critical strain may be questionable.

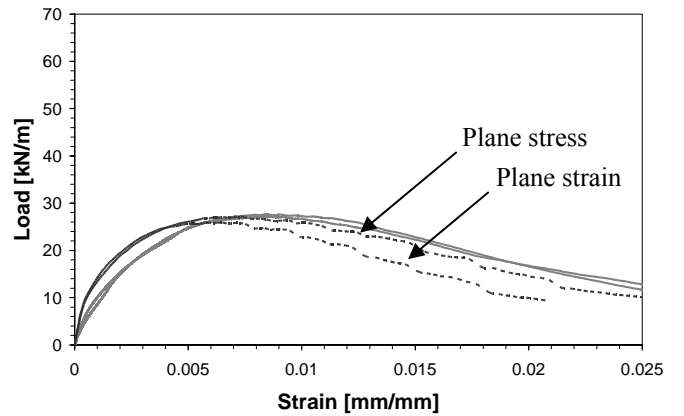


Figure 8: Load-strain curve of a notched saturated beam (notch depth 8 mm) subjected to a four-point bending test. Experimental data are indicated with solid grey lines, simulation results with dashed black lines.

#### 4 CONCLUSIONS

A general strategy to model the hygro-mechanical behavior of quasi-brittle porous materials is proposed. The new discrete constitutive equation allows for a smooth transition between the continuum state and the localized state and ensures equilibrium between the effective tractions in the undamaged material bonds and the stresses in the continuum at every stage of the failure process. The discrete equation can be used in combination with any continuum constitutive model, yielding a continuous-discontinuous material model that can describe the entire failure process. The predictive capabilities of the model crucially depend on the characteristics of the continuum model and the appropriate choice of the damage criterion. Comparison with experimental data shows that good agreement can already be obtained based on a simple mechanical model (linear elasticity) and failure criterion (Rankine).

## 5 ACKNOWLEDGEMENTS

Funding for this work was provided by the Flemish Institute for Science and Technology (IWT SBO-project IWT30175).

## REFERENCES

- Barenblatt G.I. 1962. The mathematical theory of equilibrium cracks in brittle fracture. *Advances in applied mechanics* 7: 55-129.
- Belytschko T., Black T. 1999. Elastic crack growth in finite elements with minimal remeshing. *International journal for numerical methods in Engineering* 45: 601-620.
- Carmeliet J., Van Den Abeele K.E.A. 2004. Poromechanical approach describing the moisture influence on the non-linear quasi-static and dynamic behaviour of porous building materials. *Materials and structures* 37: 271-280.
- Coussy O. 1995. *Mechanics of porous continua*. Chichester: John Wiley & Sons.
- Dolbow J., Moës N., Belytschko T. 2000. Discontinuous enrichment in finite elements with a partition of unity method. *Finite Element Analysis and Design* 36(3-4): 235-260.
- Dugdale D.S. 1960. Yielding of steel sheets containing slits. *Journal of the Mechanics and Physics of Solids* 8(2): 100-104.
- Durner W. 1994. Hydraulic conductivity estimations for soils with heterogeneous pore structure. *Water Resources Research* 30: 211-223.
- Jirásek, M. 1998. Embedded crack models for concrete fracture. In: de Borst, R. & Bicanic, N. & Mang, H. & Meschke, G. (Eds) 1998. *EURO-C 1998 Computer modeling of concrete structures*. Rotterdam: Balkema.
- Jirásek M., Zimmermann T. 2001. Embedded crack model. Part II: Combination with smeared cracks. *International Journal for Numerical Methods in Engineering* 50: 1291-1305.
- Lemaitre J. 1985. A continuous damage mechanics model for ductile fracture. *Journal of Engineering Materials and Technology* 107(1): 83-87.
- Moës N., Dolbow J., Belytschko T. 1999. A finite element method for crack growth without remeshing. *International Journal for Numerical Methods in Engineering*, 46(1): 131-150.
- Oliver J. 2000. On the discrete constitutive models induced by strong discontinuity kinematics and continuum constitutive equations. *International Journal of Solids and Structures* 37(48-50): 7207-7229.
- Oliver J., Huespe A.E., Pulido M.D.G., Chaves E. 2002. From continuum mechanics to fracture mechanics: the strong discontinuity approach. *Engineering Fracture Mechanics* 69: 113-136.
- Ren Z., Bičanić N. 1997. Simulation of progressive fracturing under dynamic loading conditions. *Communications in Numerical Methods in Engineering* 13:127-138.
- Roels S., Elsen J., Carmeliet J., Hens H. 2001. Characterisation of pore structure by combining mercury porosimetry and micrography. *Materials and Structures* 34: 76-82.
- Roels S., Moonen P., De Proft K. and Carmeliet J. 2006. A coupled discrete-continuum approach to simulate moisture effects on damage processes in porous materials. *International journal for computational methods in applied mathematics* 195(52): 7139-7153.
- Simo J.C., Ju J.W. 1987. Strain- and stress-based continuum damage models – 1. Formulation. *International journal of solids and structures* 23(7): 821-840.

- Simone A., Wells G.N., Sluys L.J. 2003. From continuous to discontinuous failure in a gradient-enhanced continuum damage model. *Computer Methods in Applied Mechanics and Engineering* 192(41-42): 4581-4607.
- Wells G.N., Sluys L.J. 2001. A new method for modelling cohesive cracks using finite elements. *International Journal of Numerical Methods in Engineering* 50: 2667-2682.